ACS OMEGA

Open Access

http://pubs.acs.org/journal/acsodf

Article

A Nanotheranostic Agent for Synergistic Antitumor Chemo/Phototherapy Prepared by Paclitaxel-Induced Self-Assembly of PEGylated Human Serum Albumin with Prolonged Circulation

Changsong Liu, Wenjia Xu, Xinlei Song,* Weilu Tian, Fuyan Liu, and Fengshan Wang*

Cite This: *ACS Omega* 2024, 9, 51062−51072

Read Online

ACCESS | Metrics & More | Article Recommendations | Supporting Information

ABSTRACT: The integration of different therapies to enhance the efficacy and minimize adverse reactions has become popular recently. This approach leverages the complementary mechanisms of action of different treatments, which can lead to better therapeutic outcomes and reduced side effects. Human serum albumin (HSA) exhibits excellent drug loading ability and is often used for biomimetic tumor delivery in multidrug nanocarriers. However, albumin nanocarriers are often unstable with a short plasma half-life. Therefore, a nanotheranostic agent for synergistic antitumor chemo/phototherapy was designed to improve HSA's pharmacokinetic properties, including prolonged circulation. Cys34-specifically PEGylated HSA (PEG-cys34HSA) was used as the nanocarrier, hydrophobic paclitaxel (PTX) served as the chemotherapeutic drug and self-assembly inducer of nanoparticles (NPs), and near-infrared dye indocyanine green (ICG) was utilized for phototherapy and fluorescence imaging. PEGylation with 20 kDa polyethylene glycol (PEG_{20kD}) promoted the formation of uniform and regular NPs more effectively than PEG_{5kD}. PEG_{20kD} also enhanced the particle size, drug loading, and encapsulation efficiency. Moreover, PEG_{20kD} significantly enhanced tumor targeting without hindering endocytosis, transport, and release of NPs. PEG_{20kD}-cys34HSA/PTX/ICG-mediated combination therapy exhibited synergistic inhibitory effects on tumor growth both *in vitro* and *in vivo*. Thus, PEG_{20kD}-cys34HSA shows potential as an alternative nanocarrier. This study provides the foundation for future investigations into PEG-modified nanocarriers and comprehensive tumor treatment.

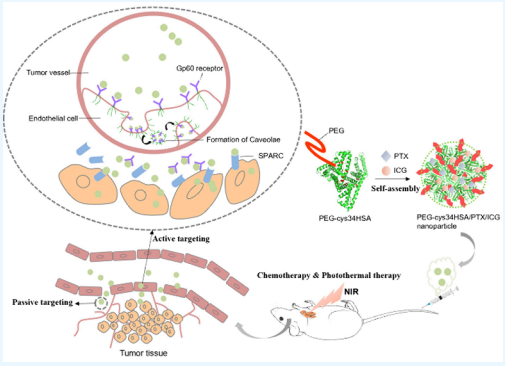

1. INTRODUCTION

Single treatment often cannot achieve optimal therapeutic efficacy due to the intricate and heterogeneous nature of tumors.[1] Multimodal combination therapy combines multiple treatments into one platform to achieve synergistic therapeutic effects while reducing drug resistance and toxic side effects. The abilities to encapsulate multiple agents and target tumors in a controlled manner have stimulated advances in nanocarrier development.[2] However, the preparation of many nanocarriers, especially inorganic materials, often involves complicated and tedious procedures. Furthermore, low metabolic rates and potential long-term toxicity may impede clinical applications of nanocarriers.[3]

Human serum albumin (HSA) plays a crucial role in transporting various natural substances in plasma.[4] HSA is suitable for multifunctional nanoplatforms due to its extraordinary binding capacity and inherent compatibility.[5−7] HSA also has an excellent tumor targeting ability, which is attributed to both passive and active targeting effects. Albumin can passively accumulate in tumor tissues due to the enhanced permeability and retention (EPR) effect. Additionally, albumin serves as a major source of energy and nutrition for rapid tumor growth.[8] Tumors express specific albumin-binding proteins, including 60 kDa glycoprotein (gp60) and SPARC (secreted protein acidic and rich in cysteine). Therefore, albumin can target tumor cells via gp60-Caveolae-SPARC transcytosis.[9,10]

Abraxane (nab-paclitaxel) is a conjugate of paclitaxel (PTX) and is approved for the treatment of non−small cell lung cancer, pancreatic cancer, and breast cancer. Abraxane exhibited remarkable efficacy and minimal adverse effects,[11] demonstrating the potential of HSA and triggered an upsurge in related research. However, abraxane was unstable and easily dissociated into individual albumin molecules in the circulation, leading to unstable drug loading, rapid drug clearance, and unintended off-target effects.[12] Furthermore, abraxane did not improve the *in vivo* half-life of PTX, and the pharmacokinetic properties of PTX, such as the area under the plasma concentration−time curve and peak concentration,

Received: June 27, 2024
Revised: October 24, 2024
Accepted: October 29, 2024
Published: December 16, 2024

were lower than those of taxol (polyoxyethyl castor oil and ethanol preparation of PTX).[13]

Polyethylene glycol (PEG), which is biocompatible, nonirritating, nontoxic, and nonimmunogenic, is the most commonly employed chemical modifier to improve the pharmacokinetic properties of protein-based biologics for human oral and intravenous administration.[14] The hydration shell of PEG protects the protein core from aggregation and phagocytosis and prolongs the systemic circulation time.[15] Hydrophobic molecules, such as PTX, can trigger the self-assembly of HSA, offering a straightforward and effective method of fabricating albumin-based nanocarriers.[5,16,17] This technique does not require the use of hazardous substances (e.g., chloroform used during preparation) or excessive energy consumption (e.g., an emulsification process by high-pressure homogenization). Notably, PEG may improve protein solubility in water-miscible organic solvents, which is conducive to self-assembly.[18,19] In addition, the large number of intermolecular hydrogen bonds in PEG support the stability of nanostructures.[20]

Currently, the most common approach to PEGylation is nonspecific amino modification at the ε-amino group of surface lysine residues and *N*-terminal amino acid residues. Although random modification is convenient, the mixed results pose challenges for separation and purification.[21] In addition, the random distribution of PEG may impede drug encapsulation, molecular interactions, and the drug release rate.[22,23] In addition, *N*-modification of proteins may alter their net charges, potentially impacting their conformation, colligative characteristics, and molecular recognition.[24,25] In contrast, site-directed modifications result in products with well-defined structures, which is advantageous for quality control.[26] HSA possesses 35 cysteine residues, but only one cysteine residue at position 34 (Cys34) is unpaired. In our previous study, we prepared Cys34-specifically PEGylated HSA (PEG-cys34HSA), which exhibited a 2.3 times longer half-life than native HSA in a rat model.[27] Cys34-PEGylation exerts negligible effects on protein conformation, PTX loading, and transport.[28,29] Thus, PEG-cys34HSA is a feasible alternative nanocarrier for drug delivery.

In the field of PEGylation, high molecular weight (MW) PEG is increasingly used to target modifications instead of randomly coupling multiple low MW PEG chains.[30] The MW of PEG is important in generating thick layers and surface shielding.[29] Increasing the MW of PEG reduces elimination and prolongs half-life.[31,32] However, PEGylation with high MW of PEG has several limitations. For instance, high MW PEG may slow the drug diffusion rate and hinder cellular transport.[31] Hence, a comprehensive evaluation of both pharmacodynamics and pharmacokinetics is essential for determining the MW of PEG.

Combining photothermal therapy (PTT) with chemotherapy has attracted attention due to the synergistic antitumor effects.[17,33] PTT usually uses near-infrared (NIR) light with excellent tissue penetration to irradiate photothermal agents and generate heat to eradicate tumor cells. As a noninvasive method, PTT has many advantages, including excellent specificity, enhanced efficiency, and reduced side effects. In addition, mild photothermal heating can increase cellular uptake, trigger drug release, and stimulate tumor-specific immune responses to augment overall anticancer efficacy.[17,34] Organic near-infrared fluorescent (NIRF) dyes, including indocyanine green (ICG), IR825, and IR820,[35−37] have gained attention as photothermal conversion materials. NIRF dyes are biocompatible and usually exhibit strong absorption in the near-infrared range. Moreover, NIRF dyes enable real-time visualization of the *in vivo* distribution to help determine optimal treatment timing. However, NIRF dyes are usually unstable and are rapidly excreted.[38] Enhancing the stability of NIRF dyes is a pivotal challenge in the development of photothermal therapies.

Albumin can combine with some NIRF dyes to form albumin−dye complexes, which increases the solubility and stability of NIRF dyes and restricts their mobility and tendency to aggregate, thereby improving the fluorescent intensity.[36,37] For example, after combining with HSA, the fluorescent intensities of ICG and IR825 increased 2-fold and 87-fold, respectively.[36,37] Therefore, efficient photothermal ablation of subcutaneous tumors can be achieved at much lower doses of HSA-IR825 (1.3 mg/kg) compared with IR825 (10 mg/kg).[37] HSA-based theranostic nanocarriers show great promise as cancer-targeted and imaging-guided combination therapies.[7,39,40]

To overcome the shortcomings of HSA as a nanocarrier (instability, short half-life, and suboptimal biodistribution), PEG-cys34HSA was used as the building block in the construction of a multifunctional nanoagent. The self-assembly of PEG-cys34HSA with PTX was induced to generate PEG-cys34HSA/PTX/ICG, an integrated nanoagent with prolonged circulation and encapsulated PTX and ICG. Under the guidance of ICG, fluorescence imaging, chemotherapy, and photothermal therapy can be administered for tumor diagnosis and treatment. Higher efficacy at a lower drug dose can be achieved to provide a long-acting, stable, biocompatible theranostic nanoagent for the comprehensive treatment of tumors.

2. MATERIALS AND METHODS

2.1. Materials. *2.1.1. Reagents.* PTX was purchased from Taxus Pharmaceutical (Jiangsu, China). ICG was obtained from Ruixi Biotechnology Co. (Xi'an, China). Monomethoxy polyethylene glycol maleimide (mPEG-MAL, MW 5 and 20 kDa) was purchased from Jiankai Biotechnology Co. (Beijing, China). HSA and trypsin were purchased from Solarbio Technology Co. (Beijing, China). Fetal bovine serum (FBS) and RPMI-1640 cell culture medium were purchased from Biological Industries (Israel). The CCK-8 assay kit was purchased from Sigma-Aldrich. All organic solvents were of analytical grade and were used without further purification.

2.1.2. Animals and Cell Lines. Mouse-derived breast cancer 4T1 cells were cryopreserved, subcultured in our laboratory, and cultured under the recommended conditions.

BALB/c mice (female, 18−20 g) were purchased from Charles River (Beijing, China). All procedures of animal experiments were approved by the Experimental Animal Ethics Review Committee of Qilu Medical College of Shandong University (approval number: 22052) and performed in accordance with the "Guiding Principles in the Care and Use of Animals (China)". Special efforts were made to minimize the use of mice in research, provide them with the most comfortable conditions, and minimize animal suffering and death. All animal carcasses are ultimately disposed of by the animal center.

2.2. Methods. *2.2.1. Preparation of PEG-cys34HSA/PTX/ICG NPs.* PEGylated HSA samples, including PEG_{5kD}-cys34HSA and PEG_{20kD}-cys34HSA, were prepared, as

https://doi.org/10.1021/acsomega.4c05986
ACS Omega 2024, 9, 51062−51072

previously described with minor modifications.[27] Detailed information can be found in the Supporting Information. Induction of hydrophobic PTX facilitated HSA and PEG-HSA assembly to form nanoparticles (NPs) encapsulating both PTX and ICG. Single-factor experiments were conducted to optimize the reaction formula, temperature, time, and stirring speed (Supporting Information). Based on the literature, HSA/PTX/ICG NPs at a molar ratio of HSA:PTX:ICG = 1:10:2 were selected as the optimal formulation. The methanol solution of PTX and the DMSO solution of ICG were added dropwise to an aqueous solution of HSA and stirred at 1000 rpm for 12 h at 10 °C. The reaction solution was centrifuged at 12,000 rpm for 10 min to remove unbound PTX and free ICG. Afterward, the HSA/PTX/ICG NPs were dialyzed with deionized water and freeze-dried.

PEG_{5kD}-cys34HSA/PTX/ICG and PEG_{20kD}-cys34HSA/PTX/ICG NPs were prepared according to the methods described above. However, the optimum molar ratio of PEG_{5kD}-cys34HSA:PTX:ICG = 1:10:2.5 and an optimum reaction temperature of 25 °C were described.

2.2.2. Characterization of NPs. The particle size and zeta potential of the NPs were evaluated by using a laser particle size analyzer. The structure and morphology of the prepared NPs were characterized by transmission electron microscopy (TEM). For the TEM analysis, HSA/PTX/ICG, PEG_{5kD}-cys34HSA/PTX/ICG, and PEG_{20kD}-cys34HSA/PTX/ICG NPs solutions at the same molar concentrations were dropped onto a 200-mesh copper mesh, dried at room temperature, and photographed using an electron microscope. An UV−Vis-NIR spectrophotometer was used to determine the concentration of PTX and ICG in the final sample, calculating the drug loading capacity and encapsulation efficiency.

2.2.3. Determination of In Vitro PTX Release. The levels of PTX released from NPs under different pH conditions were determined by using dialysis. The freeze-dried PEG_{20kD}-cys34HSA/PTX/ICG NPs (21 mg) and HSA/PTX/ICG NPs (16 mg) were suspended in 1 mL of deionized water, incubated with the dialysis membrane (MWCO = 14,000 Da), followed by incubation with 20 mL phosphate-buffered saline (PBS) at pH 5.0 or pH 7.4. The outside solution (0.4 mL) was collected at different time points (0.5, 1, 2, 4, 6, 12, 24, and 48 h) and supplemented with an equal volume of the release medium. The concentration of PTX was determined by HPLC analysis.[17]

2.2.4. Cell Experiments. The cytotoxic effects of NPs on 4T1 cancer cells *in vitro* were evaluated using a CCK-8 test kit, as previously described with slight modifications.[41] Cells were added to a 96-well plate at a seeding density of 5.0×10^3 cells/well and cultured at 37 °C for 24 h. After the culture media was discarded, the adherent cells were treated with 200 μL of different sample solutions (PTX, HSA/PTX, HSA/PTX/ICG, and PEG_{20kD}-cys34HSA/PTX/ICG) at five concentrations (1, 10, 100, 500, and 1000 nmol/mL). The control group was incubated with media only. The blank group contained CCK-8 solution and culture medium.

After the cells were incubated for 48 h, the CCK-8 assay was performed. The medicated medium was discarded and substituted with 100 μL of the fresh medium. CCK-8 solution (10 μL) was added. After the samples were incubated for 2 h, light absorption was measured at 490 nm with a microplate reader. The cell proliferation inhibition rates were calculated as follows:

$$\text{Inhibition rate (\%)} = (1 - (A_e - A_b)/(A_c - A_b)) \times 100\% \quad (1)$$

where A_e, A_b, and A_c represent the absorbance values of the experimental, blank, and control groups, respectively.

For *in vitro* combination therapy, the cells are cultured and treated in the same manner, as described above. The adherent cells were first treated with 200 μL of sample solutions (ICG, HSA/ICG, HSA/PTX/ICG, and PEG_{20kD}-cys34HSA/PTX/ICG) at five concentrations (1, 10, 100, 500, and 1000 nmol/mL) for 4 h. Subsequently, the cells were exposed to an 808 nm NIR laser at a power density of 1.0 W/cm^2 for 20 min, followed by three rinses with PBS solution. After a 24 h incubation period, the relative viability of the cells was assessed with the CCK-8 assay.

2.2.5. In Vivo Imaging and the Biological Distribution of ICG in Different NPs. The biodistribution and accumulation of NPs in tumors at designated time points after administration were monitored in a subcutaneous 4T1 tumor-bearing mouse model by using an *in vivo* optical imaging system. To establish a tumor-bearing mouse model, the armpits of mice were subcutaneously inoculated with 100 μL of a freshly harvested 1×10^7/mL 4T1 cell suspension in PBS. The Vernier scale was used to measure the dimensions of the tumor, including its length and width. The formula used to calculate the volume of the tumor was as follows:

$$V = L \times W^2/2 \quad (2)$$

where L and W represent the longest and the shortest diameters of the tumor, respectively.

After a week, when the tumor volume reached 200−300 mm^3, the mice were randomly allocated into three groups (n = 3/group). The mice were intravenously injected with free PEG_{20kD}-cys34HSA/PTX/ICG NPs, HSA/PTX/ICG NPs, or ICG through the tail-vein at an ICG dose of 0.75 mg/kg. At 1, 2, 4, 6, 8, and 24 h postinjection, the mice were anesthetized with isoflurane and the entire body was imaged using an *in vivo* fluorescence imaging apparatus. After completion of the study, mice were euthanized and the major organs, including the tumor, heart, liver, spleen, lung, and kidney, were collected to determine the ICG distribution.

2.2.6. In Vivo Antitumor Effects of Different NPs. The *in vivo* antitumor activities of different NPs under chemo/photothermal combination therapy were evaluated and compared using the subcutaneous 4T1 tumor-bearing mouse model. Five days after tumor induction, when the tumor volume reached 80 mm^3, mice were randomly allocated into six groups (n = 5/group). Mice were injected with PEG_{20kD}-cys34HSA/PTX/ICG NPs, HSA/PTX/ICG NPs, PTX, ICG, PTX+ICG, or PBS at a PTX dose of 13 mg/kg and an ICG dose of 4.6 mg/kg. The drugs were administered once every 4 days for a total of 4 doses. Four hours after administration, the tumor underwent irradiation using an 808 nm laser at a power of 1 W for 5 min. The longest and shortest diameters of the tumors were measured every 2 days, and the body weights were recorded. Mice were sacrificed by dislocation. The tumor, heart, liver, spleen, lung, and kidney of each mouse were weighed, fixed in 4% paraformaldehyde, and stained with hematoxylin−eosin (H&E) for histopathological analysis.

2.2.7. Statistical Analysis. The experimental data are presented as mean ± standard deviations (SD) and analyzed

https://doi.org/10.1021/acsomega.4c05986
ACS Omega 2024, 9, 51062−51072

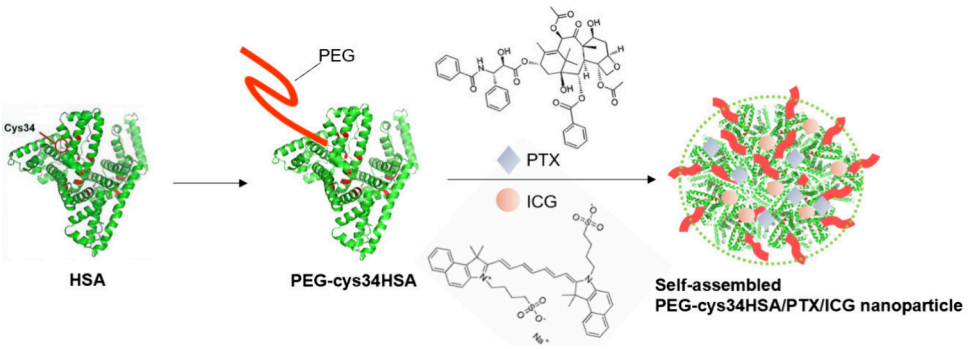

Figure 1. Schematic illustration of the formation of PEG-cys34HSA/PTX/ICG nanoparticles.

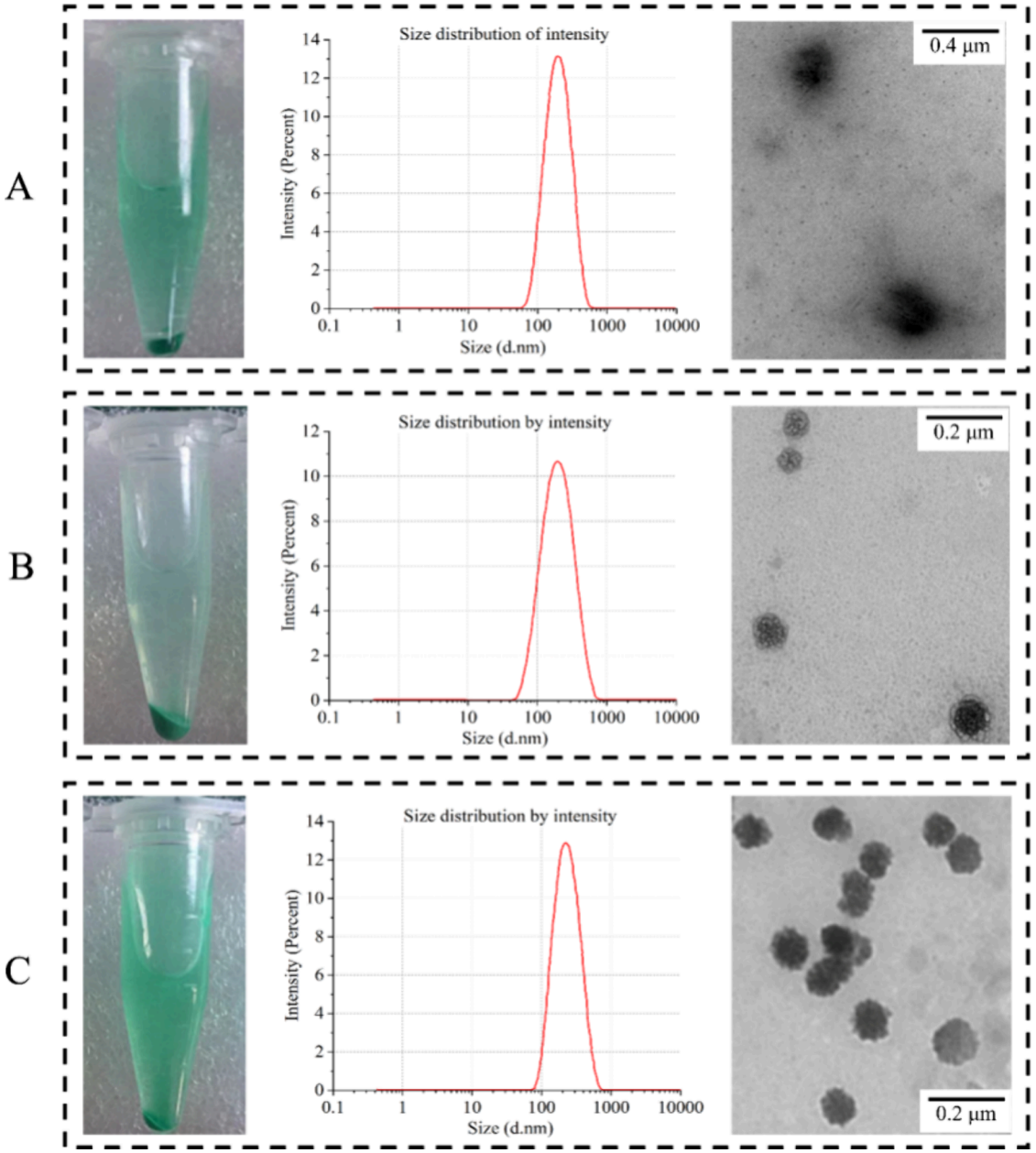

Figure 2. Characterization of nanoparticles (NPs). Left column shows photographs of the reaction solutions of NPs after stirring overnight and centrifuging. Middle column shows the particle size distribution diagrams of the NPs. Right column shows the transmission electron microscope images of the NPs. (A) HSA/PTX/ICG NPs. (B) PEG_{5kD}-cys34HSA/PTX/ICG NPs. (C) PEG_{20kD}-cys34HSA/PTX/ICG NPs.

https://doi.org/10.1021/acsomega.4c05986
ACS Omega 2024, 9, 51062−51072

Table 1. Particle Sizes and Zeta Potentials of Nanoparticles

NPs	particle size (nm)	polydispersity index (PDI)	zeta potential (mV)
HSA/PTX/ICG	158.07 ± 2.10	0.201 ± 0.011	−13.83 ± 0.500
PEG_{5kD}-cys34HSA/PTX/ICG	169.33 ± 3.36	0.179 ± 0.014	−10.29 ± 0.420
PEG_{20kD}-cys34HSA/PTX/ICG	201.00 ± 4.67	0.217 ± 0.047	−3.78 ± 0.250

Table 2. Drug Loading Capacities and Encapsulation Efficiencies of Nanoparticles

	PTX		ICG	
NPs	loading capacity (%)	encapsulation efficiency (%)	loading capacity (%)	encapsulation efficiency (%)
HSA/PTX/ICG	5.62	33.07	1.99	51.63
PEG_{5kD}-cys34HSA/PTX/ICG	2.35	15.26	0.85	23.21
PEG_{20kD}-cys34HSA/PTX/ICG	8.15	55.33	2.86	71.50

by one-way analysis of variance to determine statistical significance using SPSS software.

3. RESULTS AND DISCUSSION

3.1. Preparation and Characterization of NPs. The formation of PEG-cys34HSA/PTX/ICG NPs is illustrated in Figure 1. The particle size distribution diagrams of HSA/PTX/ICG, PEG_{5kD}-cys34HSA/PTX/ICG, and PEG_{20kD}-cys34HSA/PTX/ICG NPs are shown in the middle column of Figure 2, and the particle size and zeta potential values of NPs are summarized in Table 1. The average hydrodynamic diameters of HSA/PTX/ICG, PEG_{5kD}-cys34HSA/PTX/ICG, and PEG_{20kD}-cys34HSA/PTX/ICG were 158.07 ± 2.10, 169.33 ± 3.36, and 201.00 ± 4.67 nm, respectively. PEGylation increased the particle size of HSA NPs, especially after modification with PEG_{20kD}. The zeta potentials of HSA/PTX/ICG, PEG_{5kD}-cys34HSA/PTX/ICG, and PEG_{20kD}-cys34HSA/PTX/ICG were −13.83 ± 0.500, −10.29 ± 0.420, and −3.78 ± 0.250 mV, respectively. The absolute value of the potential of NPs decreased as the molecular weight of conjugated PEG increased. This indicates that PEG modification reduced the charge density on the surface of the NPs. The reduction in charge density can be mainly attributed to the thick hydration layer formed by PEG on the surface of NPs, which serves to shield and stabilize NPs through steric hindrance.

The drug loading capacity and encapsulation efficiency of the NPs are listed in Table 2. The PTX and ICG contents in the HSA/PTX/ICG NPs were 5.62 and 1.99%, respectively, and were similar to the previously published values.[17] However, the PTX and ICG drug loading capacity of PEG_{5kD}-cys34HSA/PTX/ICG NPs (2.35 and 0.85%) decreased compared with the drug loading capacity of HSA/PTX/ICG NPs. In contrast, the PTX and ICG loading of PEG_{20kD}-cys34HSA/PTX/ICG NPs (8.15 and 2.86%) increased compared to the drug loading capacity of HSA/PTX/ICG NPs. The influence of PEGylation on the encapsulation efficiency was the same as drug loading.

Like many other PEGylated proteins, though the pharmacokinetics and pharmacodynamics have been studied, little is known about the configuration of PEG on the surface of HSA. Initially, the PEG chain is thought to act as a flexible layer that wraps around the protein to form an external shell.[42] However, some studies suggest another dumbbell model. According to this view, the PEG chain folds upon itself in a separate random coil adjacent to the surface of the protein instead of surrounding the protein or passively extending from the surface of the protein.[43,44] In fact, many factors determine the final configuration of conjugated PEG chains. Different MW PEGs may have different spatial distributions on the protein surface, which may influence the binding of drugs to HSA and require further investigation.[45]

It can be seen from the TEM images (right column, Figure 2) that HSA/PTX/ICG NPs exhibited noticeable instability and irregular shapes. The PEG_{5kD}-cys34HSA/PTX/ICG NPs displayed a more regular shape, but their structure was less stable. In contrast, the PEG_{20kD}-cys34HSA/PTX/ICG NPs demonstrated the most regular shape and structure. These results indicated that PEGylation significantly enhanced the ability of HSA to self-assemble into NPs. Furthermore, increased PEG MW correlated with increased NP formation as well as increased size uniformity and shape regularity. These results were consistent with previous studies showing that PEGylation at Cys34 significantly increased the propensity of HSA to self-assemble into protein NPs, as characterized by the nanoparticle tracking analysis.[28] This difference may be due to the increased solubility of protein in water-miscible organic solvents and the intermolecular hydrogen bonds of PEG.

The NP reaction solutions after being stirred overnight and centrifuged are shown in the left column of Figure 2. The ICG color of the PEG_{20kD}-cys34HSA/PTX/ICG reaction solution was the darkest, followed by the HSA/PTX/ICG reaction solution, indicating that PEG_{20kD}-cys34HSA/PTX/ICG NPs carried the most ICG, followed by HSA/PTX/ICG NPs, and PEG_{5kD}-cys34HSA/PTX/ICG NPs carried the lowest ICG. These results are consistent with the drug loading results. PTX and ICG loadings of PEG_{5kD}-cys34HSA/PTX/ICG NPs were lower than those of HSA/PTX/ICG NPs. Therefore, we only investigated the targeting and antitumor effects of PEG_{20kD}-cys34HSA/PTX/ICG NPs.

3.2. *In Vitro* Release of PTX from the NPs. As shown in Figure 3, the sustained release of PTX from PEG_{20kD}-cys34HSA/PTX/ICG NPs was much slower than the release of PTX from HSA/PTX/ICG NPs. This indicates that PEGylation could enhance the stability of PTX loading in the formed HSA NPs.

The pH of PBS was set at 7.4 and 5.0 to simulate the pH in the normal tissue environment and the tumor microenvironment, respectively. Up to 48 h, the cumulative release of PTX from PEG_{20kD}-cys34HSA/PTX/ICG NPs and HSA/PTX/ICG NPs was up to 38.58 and 84.28% at pH 5.0, respectively, whereas 24.02 and 67.30% PTX has been released from the two NPs in pH 7.4 PBS in 48 h. Both NPs released PTX faster in PBS at pH 5.0 compared with the release at pH 7.4. This difference may be due to the instability of negatively charged NPs under acidic conditions and may improve tumor targeting and the effectiveness of NPs.

https://doi.org/10.1021/acsomega.4c05986
ACS Omega 2024, 9, 51062−51072

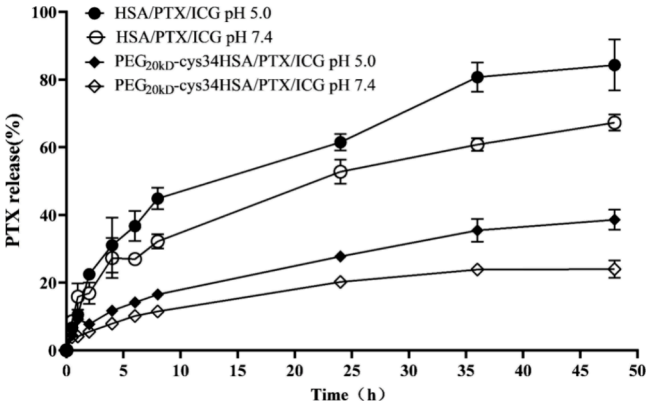

Figure 3. Cumulative release of PTX from PEG_{20kD}-cys34HSA/PTX/ICG nanoparticles (NPs) and HSA/PTX/ICG NPs *in vitro* at pH 5.0 and pH 7.4. Data are shown as mean ± SD (n = 3).

3.3. NP Cytotoxicity. In a related study,[19] HSA-PEG NPs (7−16 PEGs with MW of 5000, randomly linked to the amine groups of one HSA molecule) were delivered into the cells without losing integrity, as observed by confocal microscopy. In addition, Cys34-PEGylation with PEG_{20kD} had no negative impact on PTX transport but increased the cytotoxicity of PTX in MCF-7 cells.[29] As shown in Figure 4A, the cytotoxicity of PTX, HSA/PTX, HSA/PTX/ICG NPs, and PEG_{20kD}-cys34HSA/PTX/ICG NPs in 4T1 cancer cells increased with increasing concentrations of the drug. The inhibitory effects of the four drug treatments on cell survival were consistent. There were negligible differences in the cytotoxicities of the free PTX and NPs without laser irradiation. PEGylation did not inhibit endocytosis or transport of the NPs, and the PTX in PEG_{20kD}-cys34HSA/PTX/ICG NPs was still cytotoxic.

Figure 4B shows the relative viabilities of 4T1 cells after a 4 h incubation with different concentrations of free ICG, HSA/ICG, HSA/PTX/ICG, and PEG_{20kD}-cys34HSA/PTX/ICG NPs and irradiation with an 808 nm NIR laser at a power density of 1.0 W/cm^2 for 20 min. ICG embedded in the protein NPs exhibited significantly higher photothermal conversion efficiency compared to that of free ICG. HSA can target tumors to improve the uptake of ICG in cancer cells. In addition, HSA decreased the decomposition of ICG and enhanced the PTT. However, previous studies showed that completely killing the tumor cells with PTT only is difficult.[46,47] As shown in Figure 4B, more cell death was induced by HSA/PTX/ICG and PEG_{20kD}-cys34HSA/PTX/ICG NPs, especially at 1000 nmol/L, compared to cell death induced by phototherapy only. Thus, PTX and ICG induce obvious synergistic effects on both the HSA and the PEG_{20kD}-cys34HSA platforms. The results provide a feasible choice for efficient combination cancer therapy.

3.4. *In Vivo* Imaging and Biological Distribution of ICG for Different NPs. ICG is a fluorescent probe that can be used to monitor the distribution of NPs in real-time. The *in vivo* fluorescent tracing of free ICG and NPs in tumor-bearing mice at different time points is shown in Figure 5. The color bar from blue to red on the right implies the increase in fluorescent intensity, and the tumor sites in mice are highlighted by the dotted circle. From panel A, it can be observed that the fluorescence signal for free ICG decreased rapidly, possibly due to instability and rapid renal excretion, resulting in no accumulation of ICG in tumors. In panel C, 4 h after injection of PEG_{20kD}-cys34HSA/PTX/ICG NPs, the entire dotted circle of the tumor showed a sky blue color. At 6 and 8 h, the entire dotted circle of the tumor exhibited a predominantly dark blue tone, indicating a reduction in fluorescent intensity. This clearly demonstrated the accumulation of PEG_{20kD}-cys34HSA/PTX/ICG NPs in tumors peaked at 4 h after injection; thus, 4 h may be the best time for photothermal treatment. In contrast, panel B showed that the fluorescent intensity of HSA/PTX/ICG NPs in tumors was significantly lower than that of PEG_{20kD}-cys34HSA/PTX/ICG NPs, especially 4 h after injection. The fluorescent area of all NPs observed at 24 h was significantly reduced and even disappeared for PEG_{20kD}-cys34HSA/PTX/ICG NPs. This may be attributed to the fact that the majority of NPs were metabolized in mice at 24 h, with little left. The fluorescence of ICG and HSA NPs was predominantly localized in the liver at 24 h, especially for HSA NPs. The liver is widely recognized as the primary site for both the accumulation and elimination of NPs in drug delivery.[48] These findings suggested that PEGylation significantly reduced the level of accumulation of

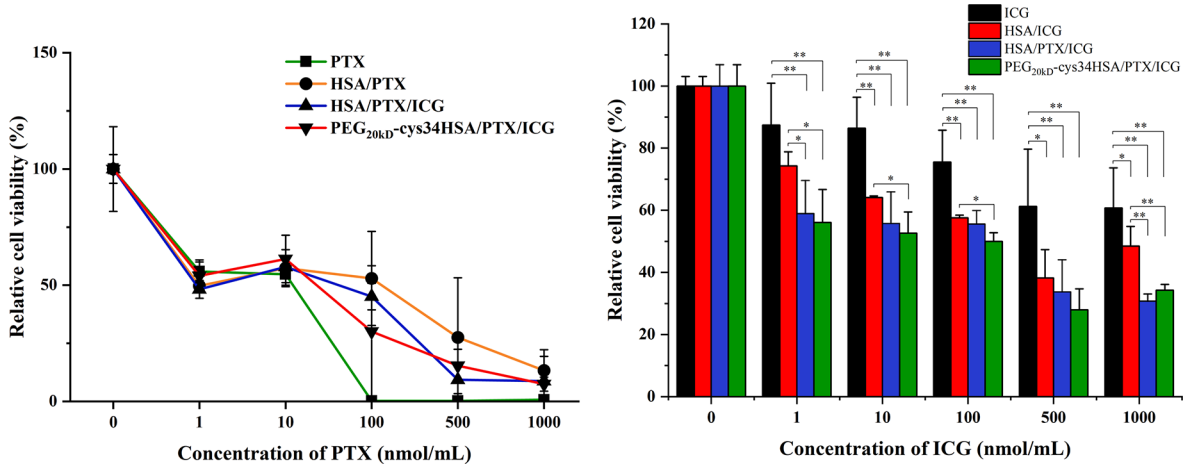

Figure 4. *In vitro* cytotoxicity of nanoparticles (NPs). (A) Relative viabilities of 4T1 cells after incubation with different concentrations of free PTX, HSA/PTX, HSA/PTX/ICG NPs, and PEG_{20kD}-cys34HSA/PTX/ICG NPs for 48 h. (B) Relative viabilities of 4T1 cells following incubation with different concentrations of free ICG, HSA/ICG, HSA/PTX/ICG NPs, and PEG_{20kD}-cys34HSA/PTX/ICG NPs for 4 h and irradiation with an 808 nm NIR laser at a power density of 1.0 W/cm^2 for 20 min. *p < 0.05, **p < 0.01. Data are shown as mean ± SD (n = 3).

https://doi.org/10.1021/acsomega.4c05986
ACS Omega 2024, 9, 51062−51072

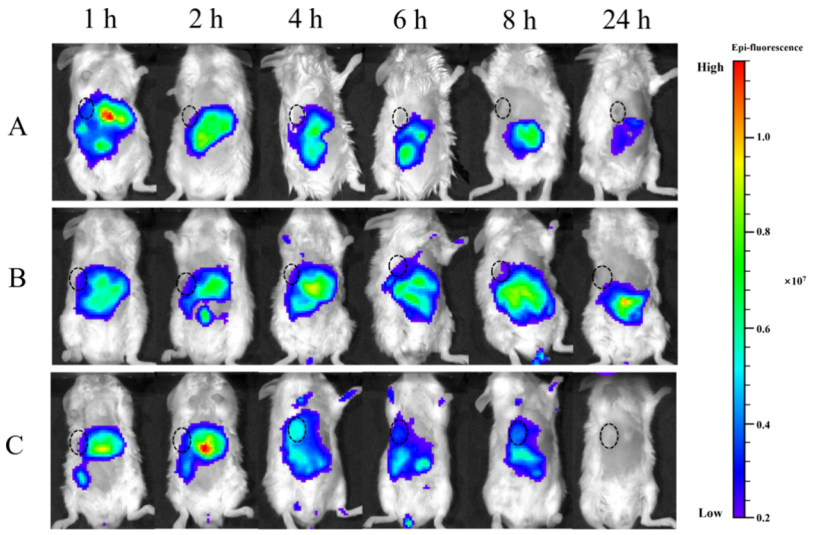

Figure 5. *In vivo* fluorescent tracing of 4T1 tumor-bearing mice captured at different time points following tail-vein injection of free ICG, HSA/PTX/ICG nanoparticles (NPs), or PEG_{20kD}-cys34HSA/PTX/ICG NPs. Dotted circle highlights the tumor sites. (A) Free ICG. (B) HSA/PTX/ICG NPs. (C) PEG_{20kD}-cys34HSA/PTX/ICG NPs.

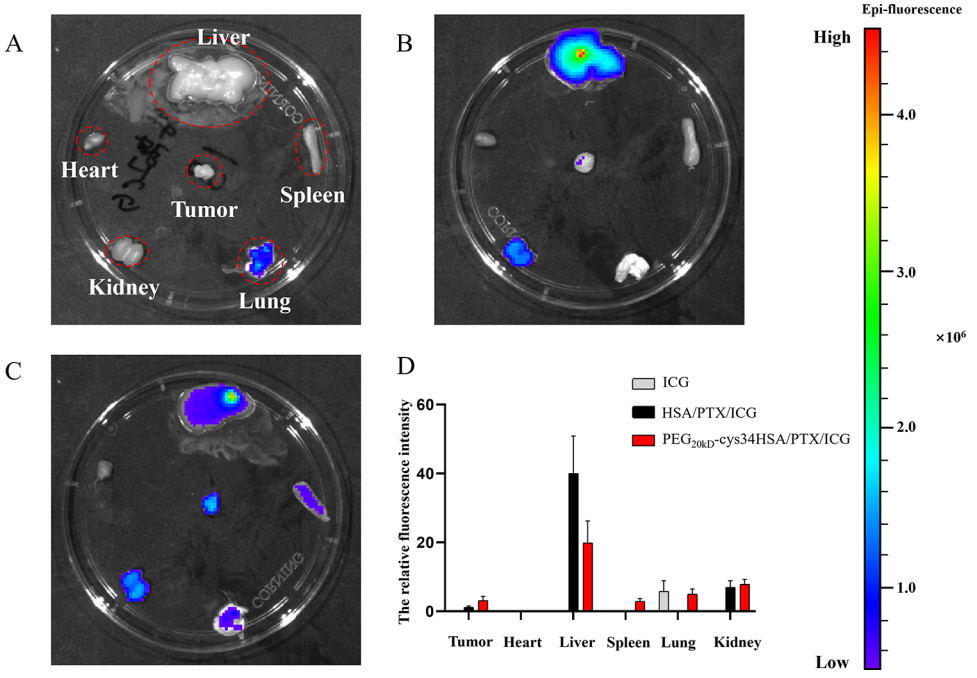

Figure 6. *Ex vivo* fluorescence images and semiquantification of fluorescence in the main organs and solid tumors from mice after intravenous tail-vein injection with free ICG, HSA/PTX/ICG nanoparticles (NPs), and PEG_{20kD}-cys34HSA/PTX/ICG NPs. (A) ICG. (B) HSA/PTX/ICG NPs. (C) PEG_{20kD}-cys34HSA/PTX/ICG NPs. (D) Semiquantitative analysis of NPs in the main organs and solid tumors as determined by fluorescence intensities.

NPs in the liver and altered the metabolism of NPs, thereby demonstrating its role in protecting proteins from phagocytosis.

Figure 6 shows the *ex vivo* fluorescent images and semiquantitative analysis of ICG in the main organs and solid tumors from mice 24 h after systemic administration. It can be seen that no ICG was retained in tumors in the free ICG group due to rapid metabolism, as mentioned previously. The fluorescent intensity of HSA/PTX/ICG NPs in liver was significantly high, consistent with Figure 5. However, the retention of HSA/PTX/ICG NPs in tumors was significantly lower than the retention of PEG_{20kD}-cys34HSA/PTX/ICG NPs. PEGylation altered the distribution of NPs within organs, enhancing tumor targeting and decreasing accumulation in the liver. Similar to liver, spleen is also a vital organ of the mononuclear scavenger system. Typically, NPs with larger diameter or a discoidal shape show splenic accumulation.[49]

Thus, the greater accumulation of PEG_{20kD}-cys34HSA/PTX/ICG in the spleen may be attributed to larger molecular weight, different shape, or extended retention *in vivo*. The results further confirmed the enhanced tumor targeting and retention of HSA by site-specific PEGylation with 20 kDa mPEG-MAL. This enhancement may be due to the increased EPR effect and half-life of the NPs, which may provide a

https://doi.org/10.1021/acsomega.4c05986
ACS Omega 2024, 9, 51062−51072

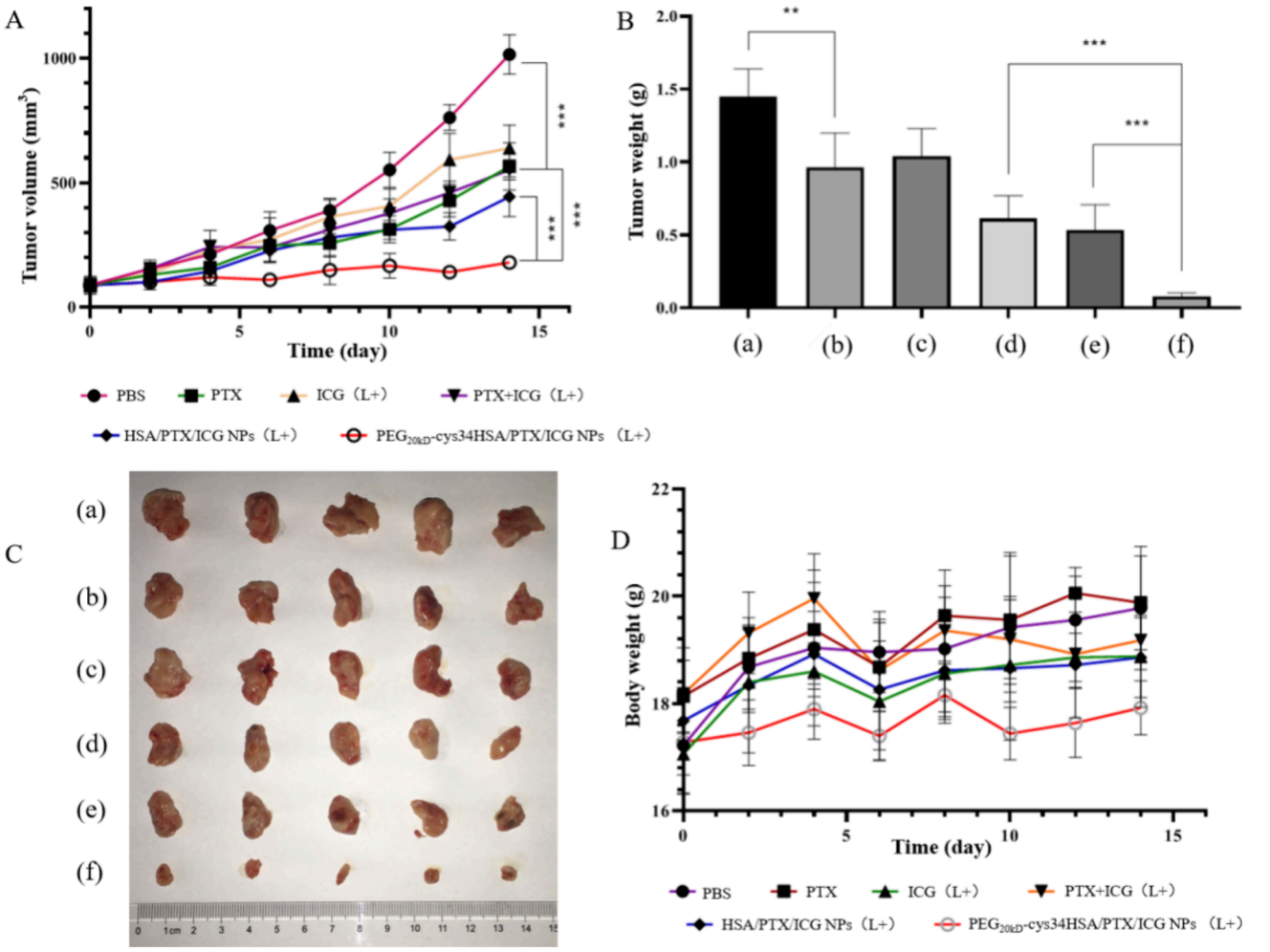

Figure 7. Effects of nanoparticles (NPs) on tumor and body weights in tumor-bearing mice. (A) Tumor growth curves. (B and C) Tumor weights and photos, respectively, after various treatments for 16 days. (D) Body weight changes. L+ refers to the 808 nm laser irradiation with a power of 1 W for 5 min. (a) PBS, (b) PTX, (c) ICG(L+), (d) PTX+ICG(L+), (e) HSA/PTX/ICG NPs (L+), and (f) PEG_{20kD}-cys34HSA/PTX/ICG NPs(L+). $^{**}p < 0.01$, $^{***}p < 0.001$.

necessary premise for improved therapeutic effects by increasing the time for interaction with the target. The fluorescence intensity of ICG is limited by tissue depth. Therefore, although the fluorescence of PEG_{20kD}-cys34HSA/PTX/ICG NPs can still be observed in organs at 24 h, it may not be detectable *in vivo* imaging in Figure 5 due to low intensity.

3.5. *In Vivo* Antitumor Effects of Different NPs. The effects of NPs on tumor and body weights of mice following different treatments are illustrated in Figure 7 (L+ refers to the 808 nm laser irradiation with a power of 1 W for 5 min). PEG_{20kD}-cys34HSA/PTX/ICG NP treatment significantly inhibited tumor growth and maintained the tumor volume at 180 mm^3 until the end of the experiment. HSA/PTX/ICG NPs (L+) treatment significantly inhibited tumor growth at an early stage, but the tumor volume increased sharply from the 8th day and grew to 450 mm^3 on the 14th day. The PEG_{20kD}-cys34HSA/PTX/ICG NPs (L+) group showed the most potent antitumor efficacy, and with an inhibition rate of 94.55%, the tumor inhibition rates in the HSA/PTX/ICG NPs (L+), PTX+ICG (L+), ICG (L+), and PTX groups were 63.15, 57.65, 28.26, and 33.50%, respectively. The tumor weight was analyzed at the end of the experiment (Figure 7B,C), constituting mutual authentication with the growth results. The synergistic chemo/photothermal antitumor effects of PEG_{20kD}-cys34HSA/PTX/ICG NPs were significantly better than the antitumor effects in other groups. The improved antitumor effects of PEG_{20kD}-cys34HSA/PTX/ICG NPs may be due to the enhanced targeting and higher retention of these NPs, as revealed by the *in vivo* imaging data. No deaths occurred during the experimental period, and mice in all groups exhibited body weight fluctuations within the expected range (Figure 7D), suggesting excellent biocompatibility of all NPs.

The extent of tumor damage and the potential organ toxicity induced by NPs were assessed using H&E staining. As shown in Figure 8, none of the NPs caused obvious toxicity in any organ, implying good targetability and biocompatibility. All groups containing ICG showed extensive tumor cell necrosis due to the photothermal effects of the 808 nm near-infrared excitation. The PEG_{20kD}-cys34HSA/PTX/ICG NPs had the most significant necrosis area, followed by HSA/PTX/ICG NPs. These results confirmed the targetability of PEG_{20kD}-cys34HSA/PTX/ICG NPs, which led to more ICG accumulation at the tumor site and higher photothermal conversion efficiency.

https://doi.org/10.1021/acsomega.4c05986
ACS Omega 2024, 9, 51062−51072

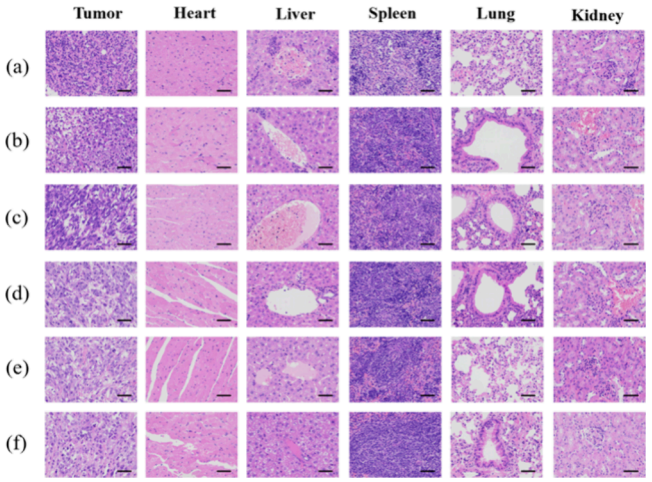

Figure 8. H&E-stained slices of mouse organs and tumors after treatment. L+ refers to the 808 nm laser irradiation with a power of 1 W for 5 min. (a) PBS, (b) PTX, (c) ICG(L+), (d) PTX+ICG(L+), (e) HSA/PTX/ICG nanoparticles (NPs) (L+), and (f) PEG_{20kD}-cys34HSA/PTX/ICG NPs(L+). Scale bars were 50 μm.

4. CONCLUSIONS

We prepared the long-circulating and image-guided chemo/photothermal therapy nanoagent PEG-cys34HSA/PTX/ICG NPs, referred to as nanotheranostic agents. The PEG-cys34HSA was prepared using covalent conjugation of PEG-MAL to the only free Cys34 of HSA. Site-specific PEGylation reduced the impact of random PEGylation on the protein structure and active sites, resulting in products with well-defined structures. PEGylation conferred significant masking properties to the protein and increased the hydrodynamic radius to increase the stability and extend the half-life of the NPs. In addition, enhanced passive EPR targeting of PEG-HSA and the tumor-targeting effects of HSA can improve the biological distribution of the drug, increasing the therapeutic effects at lower drug doses. Larger MW PEGylation improved the formation of more regular NPs with larger particle sizes. The drug loading and entrapment efficiencies of PEG_{20kD}-cys34HSA/PTX/ICG NPs were significantly increased. In contrast, the drug loading and entrapment efficiencies of PEG_{5kD}-cys34HSA/PTX/ICG were decreased. PEG_{20kD}-cys34HSA/PTX/ICG NPs had excellent tumor targeting and prominent antitumor effects both *in vitro* and *in vivo*. Therefore, PEG_{20kD}-cys34HSA is an appealing candidate for HSA as a theranostic platform for hydrophobic drugs and imaging probes. Constructing nanoagents with biocompatible materials via simple approaches, as in this study, can improve the safety of comprehensive tumor therapy. In addition, the development of bifunctional PEG and reversible PEGylation may improve targeted therapy for tumors in the future.

■ ASSOCIATED CONTENT

Supporting Information

The Supporting Information is available free of charge at https://pubs.acs.org/doi/10.1021/acsomega.4c05986.

Preparation and identification of Cys34-specifically PEGylated HSA, optimization of nanoparticle preparation methods, and single-factor experiments (PDF)

■ AUTHOR INFORMATION

Corresponding Authors

Xinlei Song − *Department of Pharmacy, Qilu Hospital, Shandong University, Jinan, Shandong 250012, China;* orcid.org/0009-0004-5634-0829; Email: xinleisong@sdu.edu.cn

Fengshan Wang − *Key Laboratory of Chemical Biology of Natural Products (Ministry of Education), Institute of Biochemical and Biotechnological Drugs, School of Pharmaceutical Sciences, Shandong University, Jinan, Shandong 250012, China;* orcid.org/0000-0002-1182-8597; Email: fswang@sdu.edu.cn

Authors

Changsong Liu − *Key Laboratory of Chemical Biology of Natural Products (Ministry of Education), Institute of Biochemical and Biotechnological Drugs, School of Pharmaceutical Sciences, Shandong University, Jinan, Shandong 250012, China*

Wenjia Xu − *Key Laboratory of Chemical Biology of Natural Products (Ministry of Education), Institute of Biochemical and Biotechnological Drugs, School of Pharmaceutical Sciences, Shandong University, Jinan, Shandong 250012, China*

Weilu Tian − *Key Laboratory of Chemical Biology of Natural Products (Ministry of Education), Institute of Biochemical and Biotechnological Drugs, School of Pharmaceutical Sciences, Shandong University, Jinan, Shandong 250012, China*

Fuyan Liu − *School of Biological Sciences and Technology, University of Jinan, Jinan 250022, China;* orcid.org/0000-0002-9905-7052

Complete contact information is available at: https://pubs.acs.org/10.1021/acsomega.4c05986

Author Contributions

Conceptualization, X.S. and F.W.; methodology, X.S. and W.X.; software, C.L. and W.T.; validation, C.L. and W.X.; formal analysis, C.L. and W.T.; investigation, W.X. and F.L.; resources, X.S. and F.L.; data curation, W.X. and F.L.; writing—original draft preparation, C.L.; writing—review and editing, X.S. and F.W.; Funding Acquisition, X.S. All authors have read and agreed to the published version of the manuscript. C.L. and W.X. contributed equally to this study.

Funding

This work was supported by the grants from the Natural Science Foundation of Shandong province (No. ZR2020QH348) and National Natural Science Foundation of China (No.82204261).

Notes

The authors declare no competing financial interest.

■ ACKNOWLEDGMENTS

The work was performed in the Institute of biochemical and biotechnological Drugs and Department of Pharmacology, School of Pharmaceutical Sciences, Shandong University.

■ REFERENCES

(1) Galon, J.; Bruni, D. Approaches to treat immune hot, altered and cold tumours with combination immunotherapies. *Nat. Rev. Drug Discovery* **2019**, *18* (3), 197−218.

(2) Shrestha, B.; Wang, L. J.; Brey, E. M.; Uribe, G. R.; Tang, L. Smart nanoparticles for chemo-based combinational therapy. *Pharmaceutics* **2021**, *13* (6), 853.
(3) Cheng, Y. J.; Hu, J. J.; Qin, S. Y.; Zhang, A. Q.; Zhang, X. Z. Recent advances in functional mesoporous silica-based nanoplatforms for combinational photo-chemotherapy of cancer. *Biomaterials* **2020**, *232*, No. 119738.
(4) Fanali, G.; di Masi, A.; Trezza, V.; Marino, M.; Fasano, M.; Ascenzi, P. Human serum albumin: From bench to bedside. *Mol. Aspects Med.* **2012**, *33* (3), 209−290.
(5) Le, X. T.; Lee, J. Y.; Nguyen, N. T.; Lee, W. T.; Lee, E. S.; Oh, K. T.; Choi, H. G.; Shin, B. S.; Youn, Y. S. Combined phototherapy with metabolic reprogramming-targeted albumin nanoparticles for treating breast cancer. *Biomater. Sci.* **2022**, *10* (24), 7117−7132.
(6) Zhang, R.; Cheng, G.; Liu, S. N.; Lv, H. Y.; Li, J. A four-in-one pure nanomedicine for synergistic multi-target therapy against breast cancer. *J. Mater. Chem. B* **2021**, *9* (42), 8809−8822.
(7) Li, C.; Wang, X.; Song, H.; Deng, S.; Li, W.; Li, J.; Sun, J. Current multifunctional albumin-based nanoplatforms for cancer multi-mode therapy. *Asian J. Pharm. Sci.* **2020**, *15* (1), 1−12.
(8) Stehle, G.; Sinn, H.; Wunder, A.; Schrenk, H. H.; Stewart, J. C. M.; Hartung, G.; MaierBorst, W.; Heene, D. L. Plasma protein (albumin) catabolism by the tumor itself-implications for tumor metabolism and the genesis of cachexia. *Crit Rev. Oncol. Hematol.* **1997**, *26* (2), 77−100.
(9) Tiruppathi, C.; Song, W.; Bergenfeldt, M.; Sass, P.; Malik, A. B. Gp60 activation mediates albumin transcytosis in endothelial cells by tyrosine kinase-dependent pathway. *J. Biol. Chem.* **1997**, *272* (41), 25968−25975.
(10) Lin, T. T.; Zhao, P. F.; Jiang, Y. F.; Tang, Y. S.; Jin, H. Y.; Pan, Z. Z.; He, H. N.; Yang, V. C.; Huang, Y. Z. Blood-brain-barrier-penetrating albumin nanoparticles for biomimetic drug delivery *via* albumin-binding protein pathways for antiglioma therapy. *ACS Nano* **2016**, *10* (11), 9999−10012.
(11) Gradishar, W. J. Albumin-bound paclitaxel: a next-generation taxane. *Expert Opin. Pharmacother.* **2006**, *7* (8), 1041−1053.
(12) Li, C. L.; Li, Y. H.; Gao, Y. Q.; Wei, N.; Zhao, X.; Wang, C. X.; Li, Y. F.; Xiu, X.; Cui, J. X. Direct comparison of two albumin-based paclitaxel-loaded nanoparticle formulations: Is the crosslinked version more advantageous? *Int. J. Pharm.* **2014**, *468* (1−2), 15−25.
(13) Sparreboom, A.; Scripture, C. D.; Trieu, V.; Williams, P. J.; De, T. P.; Yang, A.; Beals, B.; Figg, W. D.; Hawkins, M.; Desai, N. Comparative preclinical and clinical pharmacokinetics of a cremophor-free, nanoparticle albumin-bound paclitaxel (ABI-007) and paclitaxel formulated in cremophor (Taxol). *Clin. Cancer. Res.* **2005**, *11* (11), 4136−4143.
(14) Ryan, S. M.; Mantovani, G.; Wang, X. X.; Haddleton, D. M.; Brayden, D. J. Advances in PEGylation of important biotech molecules: delivery aspects. *Expert. Opin. Drug. Del.* **2008**, *5* (4), 371−383.
(15) Meng, W.; Guo, X. L.; Qin, M.; Pan, H.; Cao, Y.; Wang, W. Mechanistic insights into the stabilization of srcSH3 by PEGylation. *Langmuir* **2012**, *28* (46), 16133−16140.
(16) Chen, Q.; Liu, X. D.; Zeng, J. F.; Cheng, Z. P.; Liu, Z. Albumin-NIR dye self-assembled nanoparticles for photoacoustic pH imaging and pH-responsive photothermal therapy effective for large tumors. *Biomaterials* **2016**, *98*, 23−30.
(17) Chen, Q.; Liang, C.; Wang, C.; Liu, Z. An imagable and photothermal "Abraxane-like" nanodrug for combination cancer therapy to treat subcutaneous and metastatic breast tumors. *Adv. Mater.* **2015**, *27* (5), 903−910.
(18) Inada, Y.; Takahashi, K.; Yoshimoto, T.; Ajima, A.; Matsushima, A.; Saito, Y. Application of polyethylene glycol-modified enzymes in biotechnological processes- organic solvent-soluble enzymes. *Trends Biotechnol.* **1986**, *4* (7), 190−194.
(19) Lee, J. E.; Kim, M. G.; Jang, Y. L.; Lee, M. S.; Kim, N. W.; Yin, Y.; Lee, J. H.; Lim, S. Y.; Park, J. W.; Kim, J.; et al. Self-assembled PEGylated albumin nanoparticles (SPAN) as a platform for cancer chemotherapy and imaging. *Drug Delivery* **2018**, *25* (1), 1570−1578.
(20) Kim, S. H.; Tan, J. P. K.; Nederberg, F.; Fukushima, K.; Colson, J.; Yang, C. A.; Nelson, A.; Yang, Y. Y.; Hedrick, J. L. Hydrogen bonding-enhanced micelle assemblies for drug delivery. *Biomaterials* **2010**, *31* (31), 8063−8071.
(21) Hamidi, M.; Azadi, A.; Rafiei, P. Pharmacokinetic consequences of pegylation. *Drug Delivery* **2006**, *13* (6), 399−409.
(22) Kouchakzadeh, H.; Shojaosadati, S. A.; Maghsoudi, A.; Farahani, E. V. Optimization of PEGylation Conditions for BSA nanoparticles using response surface methodology. *AAPS PharmSciTech* **2010**, *11* (3), 1206−1211.
(23) Lin, W.; Garnett, M. C.; Davis, S. S.; Schacht, E.; Ferruti, P.; Illum, L. Preparation and characterisation of rose Bengal-loaded surface-modified albumin nanoparticles. *J. Controlled Release* **2001**, *71* (1), 117−126.
(24) Gao, J. P.; Yong, Z. H.; Zhang, F.; Ruan, K. C.; Xu, C. H.; Chen, G. Y. Positive charges on lysine residues of the extrinsic 18 kDa protein are important to its electrostatic interaction with spinach photosystem II membranes. *Acta Biochim. Biophys. Sin.* **2005**, *37* (11), 737−742.
(25) Broersen, K.; Weijers, M.; de Groot, J.; Hamer, R. J.; de Jongh, H. H. J. Effect of protein charge on the generation of aggregation-prone conformers. *Biomacromolecules* **2007**, *8* (5), 1648−1656.
(26) Nischan, N.; Hackenberger, C. P. R. Site-specific PEGylation of proteins: Recent developments. *J. Org. Chem.* **2014**, *79* (22), 10727−10733.
(27) Zhao, T.; Cheng, Y. N.; Tan, H. N.; Liu, J. F.; Xu, H. L.; Pang, G. L.; Wang, F. S. Site-Specific chemical modification of human serum albumin with polyethylene glycol prolongs half-life and improves intravascular retention in mice. *Biol. Pharm. Bull.* **2012**, *35* (3), 280−288.
(28) Mehtala, J. G.; Kulczar, C.; Lavan, M.; Knipp, G.; Wei, A. Cys34-PEGylated human serum albumin for drug binding and delivery. *Bioconjugate Chem.* **2015**, *26* (5), 941−949.
(29) Plesner, B.; Fee, C. J.; Westh, P.; Nielsen, A. D. Effects of PEG size on structure, function and stability of PEGylated BSA. *Eur. J. Pharm. Biopharm.* **2011**, *79* (2), 399−405.
(30) Roberts, M. J.; Bentley, M. D.; Harris, J. M. Chemistry for peptide and protein PEGylation. *Adv. Drug Delivery Rev.* **2012**, *64*, 116−127.
(31) Miteva, M.; Kirkbride, K. C.; Kilchrist, K. V.; Werfel, T. A.; Li, H. M.; Nelson, C. E.; Gupta, M. K.; Giorgio, T. D.; Duvall, C. L. Tuning PEGylation of mixed micelles to overcome intracellular and systemic siRNA delivery barriers. *Biomaterials* **2015**, *38*, 97−107.
(32) Cui, J. W.; De Rose, R.; Alt, K.; Alcantara, S.; Paterson, B. M.; Liang, K.; Hu, M.; Richardson, J. J.; Yan, Y.; Jeffery, C. M.; et al. Engineering poly(ethylene glycol) particles for improved biodistribution. *ACS Nano* **2015**, *9* (2), 1571−1580.
(33) Thangudu, S.; Kaur, N.; Korupalli, C.; Sharma, V.; Kalluru, P.; Vankayala, R. Recent advances in near infrared light responsive multifunctional nanostructures for phototheranostic applications. *Biomater. Sci.* **2021**, *9* (16), 5472−5483.
(34) Yu, Q. W.; Tang, X.; Zhao, W.; Qiu, Y.; He, J.; Wan, D. D.; Li, J. P.; Wang, X. H.; He, X.; Liu, Y. Y.; et al. Mild hyperthermia promotes immune checkpoint blockade-based immunotherapy against metastatic pancreatic cancer using size-adjustable nanoparticles. *Acta Biomater.* **2021**, *133*, 244−256.
(35) Zhang, D.; Zhang, J.; Li, Q.; Tian, H. L.; Zhang, N.; Li, Z. H.; Luan, Y. X. pH- and enzyme-sensitive IR820-paclitaxel conjugate self-assembled nanovehicles for near-infrared fluorescence imaging-guided chemo-photothermal therapy. *ACS Appl. Mater. Interfaces.* **2018**, *10* (36), 30092−30102.
(36) Sheng, Z. H.; Hu, D. H.; Zheng, M. B.; Zhao, P. F.; Liu, H. L.; Gao, D. Y.; Gong, P.; Gao, G. H.; Zhang, P. F.; Ma, Y. F.; et al. Smart human serum albumin-indocyanine green nanoparticles generated by programmed assembly for dual-modal imaging-guided cancer synergistic phototherapy. *ACS Nano* **2014**, *8* (12), 12310−12322.
(37) Chen, Q.; Wang, C.; Zhan, Z. X.; He, W. W.; Cheng, Z. P.; Li, Y. Y.; Liu, Z. Near-infrared dye bound albumin with separated

https://doi.org/10.1021/acsomega.4c05986
ACS Omega 2024, 9, 51062−51072

imaging and therapy wavelength channels for imaging-guided photothermal therapy. *Biomaterials* **2014**, *35* (28), 8206−8214.
(38) Kirchherr, A. K.; Briel, A.; Mäder, K. Stabilization of indocyanine green by encapsulation within micellar systems. *Mol. Pharmaceutics.* **2009**, *6* (2), 480−491.
(39) Park, S.; Kim, H.; Lim, S. C.; Lim, K.; Lee, E. S.; Oh, K. T.; Choi, H. G.; Youn, Y. S. Gold nanocluster-loaded hybrid albumin nanoparticles with fluorescence-based optical visualization and photothermal conversion for tumor detection/ablation. *J. Controlled Release* **2019**, *304*, 7−18.
(40) Ma, H. S.; Yang, X. Q.; Ke, J.; Wang, C.; Peng, L. J.; Hu, F. Q.; Yuan, H. Smart assembled human serum albumin nanocarrier enhanced breast cancer treatment and antitumor immunity by chemo-photothermal Therapy. *ACS Biomater. Sci. Eng.* **2020**, *6* (5), 3217−3229.
(41) Yang, X. Y.; Shi, X. Q.; Zhang, Y. A.; Xu, J. K.; Ji, J. B.; Ye, L.; Yi, F.; Zhai, G. X. Photo-triggered self-destructive ROS-responsive nanoparticles of high paclitaxel/chlorin e6 co-loading capacity for synergetic chemo-photodynamic therapy. *J. Controlled Release* **2020**, *323*, 333−349.
(42) Lu, Y. L.; Harding, S. E.; Turner, A.; Smith, B.; Athwal, D. S.; Grossmann, J. G.; Davis, K. G.; Rowe, A. J. Effect of PEGylation on the solution conformation of antibody fragments. *J. Pharm. Sci.* **2008**, *97* (6), 2062−2079.
(43) Pai, S. S.; Hammouda, B.; Hong, K. L.; Pozzo, D. C.; Przybycien, T. M.; Tilton, R. D. The conformation of the poly(ethylene glycol) chain in mono-PEGylated Lysozyme and mono-PEGylated human growth hormone. *Bioconjugate Chem.* **2011**, *22* (11), 2317−2323.
(44) He, L. Z.; Wang, H.; Garamus, V. M.; Hanley, T.; Lensch, M.; Gabius, H. J.; Fee, C. J.; Middelberg, A. Analysis of monoPEGylated human galectin-2 by small-angle X-ray and neutron scattering: Concentration dependence of PEG conformation in the conjugate. *Biomacromolecules* **2010**, *11* (12), 3504−3510.
(45) Shu, J. Y.; Lund, R.; Xu, T. Solution structural characterization of coiled-coil peptide-polymer side-conjugates. *Biomacromolecules* **2012**, *13* (6), 1945−1955.
(46) Yu, L. X.; Dong, A. J.; Guo, R. W.; Yang, M. Y.; Deng, L. D.; Zhang, J. H. DOX/ICG coencapsulated liposome-coated thermosensitive nanogels for NIR-triggered simultaneous drug release and photothermal effect. *ACS Biomater. Sci. Eng.* **2018**, *4* (7), 2424−2434.
(47) Peng, J. R.; Xiao, Y.; Li, W. T.; Yang, Q.; Tan, L. W.; Jia, Y. P.; Qian, Z. Y. Photosensitizer micelles together with IDO inhibitor enhance cancer photothermal therapy and immunotherapy. *Adv. Sci.* **2018**, *5* (5), No. 1700891.
(48) Kim, J.; Eygeris, Y.; Ryals, R. C.; Jozic, A.; Sahay, G. Strategies for non-viral vectors targeting organs beyond the liver. *Nat. Nanotechnol.* **2024**, *19* (4), 428−447.
(49) Blanco, E.; Shen, H.; Ferrari, M. Principles of nanoparticle design for overcoming biological barriers to drug delivery. *Nat. Biotechnol.* **2015**, *33* (9), 941−951.

https://doi.org/10.1021/acsomega.4c05986
ACS Omega 2024, 9, 51062−51072